RESEARCH ARTICLE

A Robust Passive Islanding Detection Technique With Zero-Non-Detection Zone for Inverter-Interfaced Distributed Generation

B. PANGEDAIAH[1]**, P. L. SANTOSH KUMAR REDDY**[2]**, Y. P. OBULESU**[2]**,
VENKATA REDDY KOTA**[3]**, (Senior Member, IEEE),
AND MAMDOUH L. ALGHAYTHI**[4]**, (Member, IEEE)**
[1]Electrical and Electronics Engineering Department, Lakireddy Bali Reddy College of Engineering, Mylavaram, Andhra Pradesh 533003, India
[2]School of Electrical Engineering, Vellore Institute of Technology, Vellore, Tamil Nadu 632014, India
[3]Electrical and Electronics Engineering Department, JNTUK, Kakinada, Andhra Pradesh 533003, India
[4]Department of Electrical Engineering, College of Engineering, Jouf University, Sakaka, Al-Jouf 72388, Saudi Arabia

Corresponding authors: B. Pangedaiah (pangedaiah@gmail.com) and Mamdouh L. Alghaythi (mlalghaythi@ju.edu.sa)

This work was supported by the Deanship of Scientific Research at Jouf University under Grant DSR-2021-02-0302.

ABSTRACT In this paper, a new and efficient passive islanding detection technique for a grid-connected hybrid distributed generating system has been proposed using Second Generation Wavelet Transform (SGWT) and Maximum Overlap Discrete Wavelet Transform (MODWT). In this technique, the ripple content of the voltage signal is measured at the Point of Common Coupling (PCC) and it is monitored through the decomposition of the signal by applying SGWT and MODWT technique up to suitable finer levels. This algorithm able to detects all kinds of islanding at nearly 0.3 sec, even with zero power mismatch. It is verified on a wide range of operational conditions and is also validated in various non-islanding conditions. Furthermore, the proposed technique is simple, there is no need for a classifier requirement, not depends on system parameters, zero non-detection zone (NDZ), and its operation is independent of the capacity and nature of distributed generation (DG) connected to the utility grid.

INDEX TERMS Grid connected distributed generation, maximum overlap discrete wavelet transform, passive islanding detection, second generation wavelet transform, time domain analysis, zero-non-detection zone.

I. INTRODUCTION

A. MOTIVATION

The accelerated degradation of traditional energy supplies and increasing emissions levels have driven researchers to focus on accessible renewable energy sources. Globally, renewable energy sources such as wind and solar photovoltaic (P.V.) system-based power generation are strongly promoted. These sources are widespread in the harvesting domains of residential and industrial areas. There have been many installations of renewable power sources over the past couple of years, so the wind and solar P.V. power generation

prices have declined sharply. The superior task is integrating renewable energy sources with the utility grid and protecting D.G. systems against unintentional islanding. As per IEEE standard 1547-2018, if a D.G. system is isolated from the grid when breaker isolation, a part of the power system becomes continually energized from the D.G. Islanding harm infrastructure and power quality problems related to voltage and frequency fluctuations in the D.G. system's connection to the grid. As a result, islanding is always quickly identified [1], [2] to safeguard electrical devices and the D.G.

B. LITERATURE REVIEW

Islanding detection techniques may be classified generally into passive, active, and communication-based approaches.

The associate editor coordinating the review of this manuscript and approving it for publication was Chandan Kumar.

Each approach has several merits and limitations. However, these are the most often used strategies for islanding detection. The communication-based approach delivers better outcomes without altering the efficiency of the power system network. Additionally, considering its high cost and complex processes, the decreased NDZ benefits [3]. Active methods can detect islanding when deliberately injecting perturbations into the D.G. unit. Active approaches introduce power quality issues that affect the power system's efficiency, even though it appears to be a small NDZ [4]. Passive methods are concerned, even though the passive methods are well developed. Still, they rely on continuous measurement of system parameters such as variation in the voltage, frequency, harmonic distortion, etc. By setting specific threshold values for the system parameters, islanding and non-islanding cases can be differentiated [5]. Various passive islanding detection techniques are available in the literature, including conventional, signal processing, and intelligent techniques. The most often employed passive islanding detection approaches are dependent on voltage and frequency components that are either under or over. The rate in change of voltage or frequency shift was used to monitor the islanding. The effectiveness of the passive islanding detection techniques could be increased by using more responsive indications such as rate of change of frequency, rate of change of reactive power, voltage unbalances, total harmonic distortion, and oscillation frequency estimation, etc. However, they may fail to predict the islanding condition whenever the local load matches the D.G. power. Later, the islanding detection strategies focused on modern signal processing techniques for quick and accurate detection. S-transforms [6], [7] provide multi-resolution analysis that is insensitive to signal-to-noise ratios. Nonetheless, it takes more computing time, and the computational complexity increases significantly for transient situations and harmonic distortion, reducing the islanding detection's efficiency. The wavelet transform seems useful for evaluating non-stationary signals whose frequency changes with time. It provides information on time to derive transient information through the frequency component of non-stationary signals [8], [9]. The DWT has a disadvantage of limitation of signal length, i.e., multiple-power-of-two, and lack of translation-invariance. Data processing is carried out in DWT using a memory-intensive algorithm, which requires a convolution and filtering operation. So, the computational difficulty increases as the length of the filter increases. The DWT requires high computational time, more memory, and sensitivity for selecting a signal starting position. Empirical Mode Decomposition (EMD) [10], Orthogonal EMD (OEMD) [11], Variational-Mode Decomposition (VMD) [12], Transient Monitoring Function (TMF) [13], Mathematical Morphology (MM) [14] and Matrix Pencil (MP) [15] algorithms were also used for islanding detection. These algorithms perform better compared to the above-discussed techniques, but these methods still have certain limitations. The EMD and OEMD approaches were having a problem with mode mixing, whereas the TMF and MM

algorithm's performance reduces with a rise in noise levels. Apart from the limitations mentioned above in islanding detection algorithms using signal processing techniques, some techniques require a classifier to distinguish islanding and non-islanding cases; this raises the computational burden of the algorithm. Some algorithms do not require any classifier, but they will work by setting the threshold. While setting the threshold for non-islanding situations, proper care should be taken such that the deviations are always lower than the threshold values. It may fail to detect islanding when considering full ranges of non-islanding events. Therefore, there is a need for an effective signal decomposition approach in passive islanding detection methods.

C. CONTRIBUTION AND ORGANIZATION OF THE PAPER

During islanding, the lack of stability of the grid can cause an unexpected and persistent change in the amplitude of the voltage at the PCC, which can be used to detect the islanding. In this paper, to overcome the limitations in the existing techniques, two new techniques are proposed for islanding detection: SGWT and MODWT. The proposed techniques detect the islanding by considering the lower frequency components of the PCC voltage signal. These techniques have no NDZ limitation, even when load power matches the D.G. power and effectively separates the non- islanding and islanding cases without any classifier. The following are the main contributions of this paper: i) The suggested criterion could rapidly recognize the distinction between the islanded mode and the grid-connected mode, even when demand and generation are perfectly matched. Because of this, the proposed islanding detection criteria have no NDZ, which is different from passive detection approaches. ii) Identifies islanding under dynamic loading scenarios and differentiates accurately between non-islanding and islanding conditions without the need for a classifier. iii) Selecting a single threshold value that obviates the requirement for adaptive thresholds in a range of operational conditions. The proposed work is implemented using MATLAB / Simulink and OPAL-RT Real-Time Hardware-in-Loop (HIL) simulator environment.The proposed methods are being tested for different operating conditions, and their effectiveness is verified through simulation and HIL results.

This paper is organized as follows: Section 2 illustrates the determination of wavelet coefficients using SGWT and MODWT. The description of the hybrid D.G. system and algorithm of the proposed method is presented in section 3. Section 4 gave the results and discussion of the proposed approach. Finally, conclusions are provided in Section 5.

II. CALCULATION OF WAVELET COEFFICIENTS
A. SECOND GENERATION WAVELET TRANSFORMATION (SGWT)
The fast and straightforward SGWT solution is ideal for islanding detection. The SGWT's low memory requirement and lower computational time properties make it significant
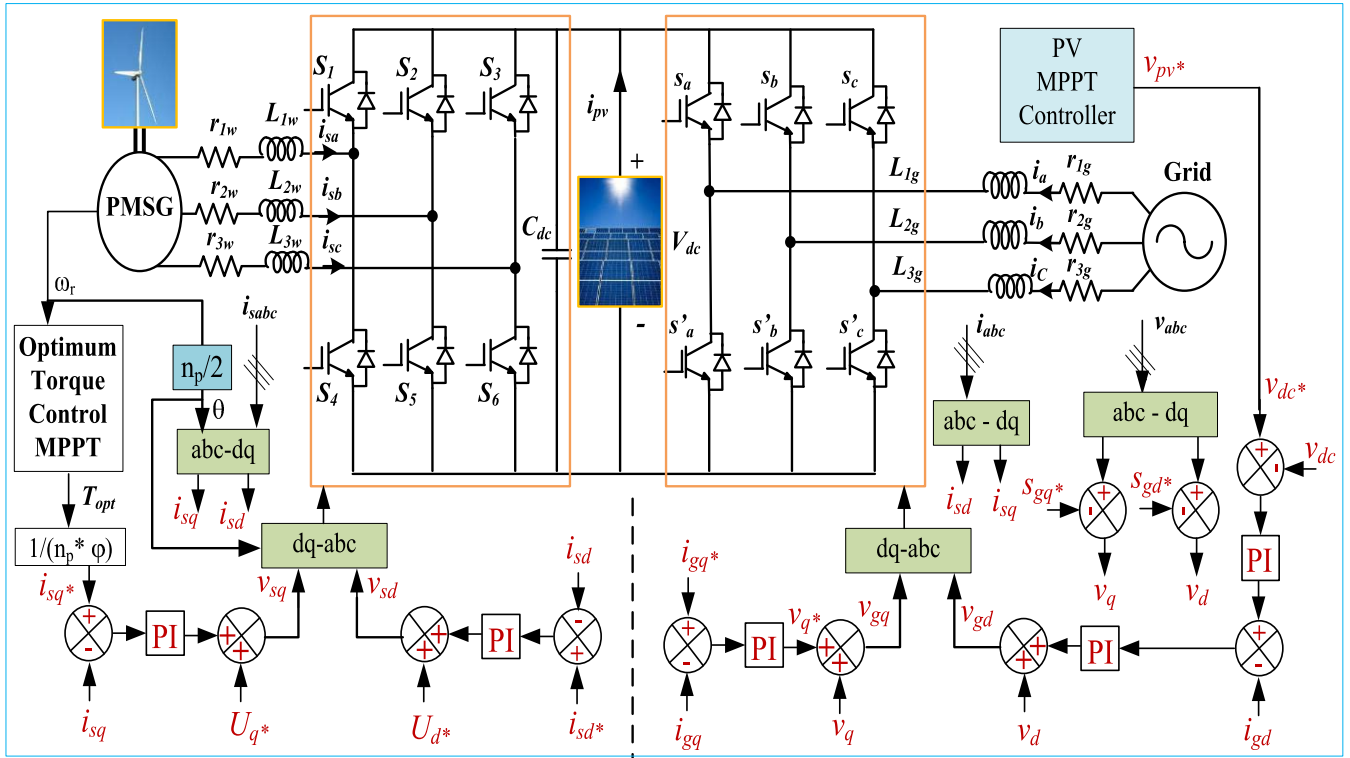
FIGURE 1. Block diagram of the PMSG-PV hybrid system.

in detecting islanding. The Lifting Scheme (L.S.) in the SGWT decreases the number of unnecessary computations of DWT. The L.S. is more versatile than the wavelet in design and execution [16]. The following three steps were included in the lifting wavelet scheme adopted on a voltage signal $Y[n]$ with 'n' samples to convert into an approximation signal '$a[n]'$ and a detailed signal '$d[n]'$ as follows:

Split: The voltage signal, Y[n] split into two disjoint sub-sets, that is $Y_{even}[n] = E[n]$, even indexed samples, and $Y_{odd}[n] = O[n]$, odd indexed samples, which are strongly correlated. This correlation mechanism is local.

$$Y[n] = E[n] + O[n] \qquad (1)$$

Predict: This step is used to generate detailed coefficients d[n] of the signal $Y[n]$ from the decomposition of the wavelet using Eq. 2 given below. Prediction Operator (P) is a linear combination of neighboring even indexed samples.

$$d[n] = O[n] - P(E[n]) \qquad (2)$$

Update: The approximation coefficients a[n] of the initial signal Y[n] are estimated using Eq. 3. It updates the even components based on a linear combination of different samples collected from the predicted step. Update operator (U) is a linear combination of the neighboring detailed coefficient values.

$$a[n] = E[n] - U(d[n]) \qquad (3)$$

First-level approximations have been used to iterate the operation. The SGWT needs half the number of computations compared to the traditional convolution-based Wavelet transforms.

B. MAXIMUM OVERLAP DISCRETE WAVELET TRANSFORMATION (MODWT)

It also has a decomposition of the original signal based on the quadrature of the mirror filter, which separates the frequency spectrum, and the coefficients of scale and wavelet are extracted at the output of every filter. The critical distinction between MODWT and DWT is that in the DWT, the number of samples of the signal decreases at each level of decomposition, whereas in MODWT, it preserves the signal's length. There is no limit on the signal size in the MODWT, unlike the standard DWT. So, for all signal lengths, the MODWT may be implemented. By eliminating down-sampling, the tolerance to the first selection position can be reduced. The MODWT can be used for any section 'N' with an integer multiple of '2^j'for j = 1, 2, 3, ..., J, where 'j' is the scale, and J is the decomposition level of the MODWT [17]. The Eq. 4 and 5 give the MODWT scaling coefficients $\widetilde{V}_j$ and the wavelet coefficient $\widetilde{W}_j$ at the 'n^{th},' element of the 'j^{th},' stage with the input signal $Y(n)$ and scaling filter $\widetilde{h}_1$ and wavelet filter $\widetilde{g}_1$ of the MODWT.

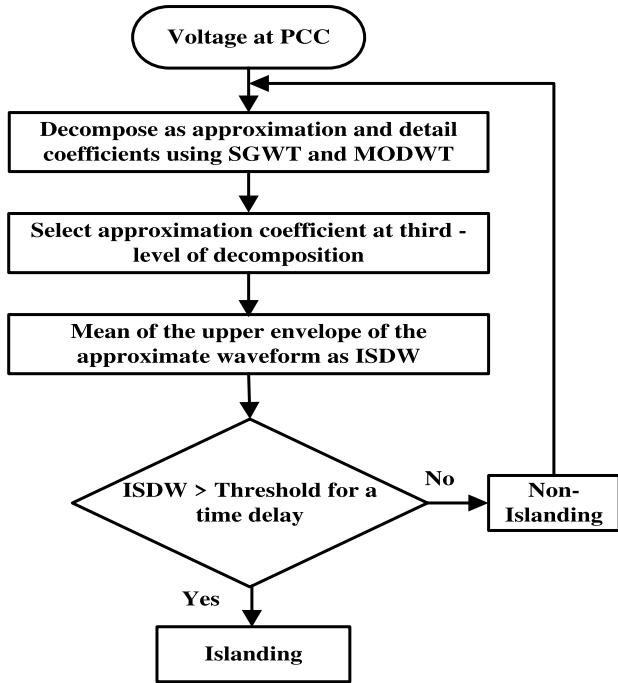$$\widetilde{V}_{j,n} = \sum_{k=0}^{L_j - 1} \widetilde{g}_{j,1} \widetilde{Y}_{n-1} mod N \qquad (4)$$

FIGURE 2. Flowchart for the proposed algorithm of SGWT and MODWT.

FIGURE 3. (a) Single-phase voltage at PCC (b) approximate coefficients (c) ISDW.

$$\widetilde{W}_{j,n} = \sum_{k=0}^{L_j-1} \widetilde{h}_{j,1} \widetilde{Y}_{n-1} mod N \tag{5}$$

where n=1,2,3,..., N. N is the length of the signal, k= 0,1,2,...,L-1. L is the filter length. The Eq. 6 and 7 provide the approximations $\widetilde{A}_j$ and the details $\widetilde{D}_j$) of the nth element of a jth stage of the MODWT.

$$\widetilde{A}_{j,n} = \sum_{k=0}^{L_j-1} \widetilde{g}_{j,k}^0 \widetilde{V}_{n+k} mod N \tag{6}$$

$$\widetilde{D}_{j,n} = \sum_{k=0}^{L_j-1} \widetilde{h}_{j,k}^0 \widetilde{W}_{n-1} mod N \tag{7}$$

where $\widetilde{g}^0$ and $\widetilde{h}^0$ periodized $\widetilde{g}$ and $\widetilde{h}$ to length N. In terms of approximations and details, the original time series signal Y(n) can be expressed as shown in Eq. 8.

$$Y(n) = \sum_{k=0}^{j} (\widetilde{D}_j) + \widetilde{A}_j \tag{8}$$

III. TEST SYSTEM AND PROPOSED METHOD

A. ARCHITECTURE AND CONTROL SCHEME

The test system consists of a wind turbine connected to a Wind Side Converter (WSC), and a grid-connected Grid Side Converter (GSC). A dc-link capacitor connects the photovoltaic array directly to the back-to-back voltage source converter. Both the WSC [18] and GSC [19] are six-cell converters consisting of an IGBT switch. The block diagram of the proposed wind turbine fed PMSG-PV hybrid
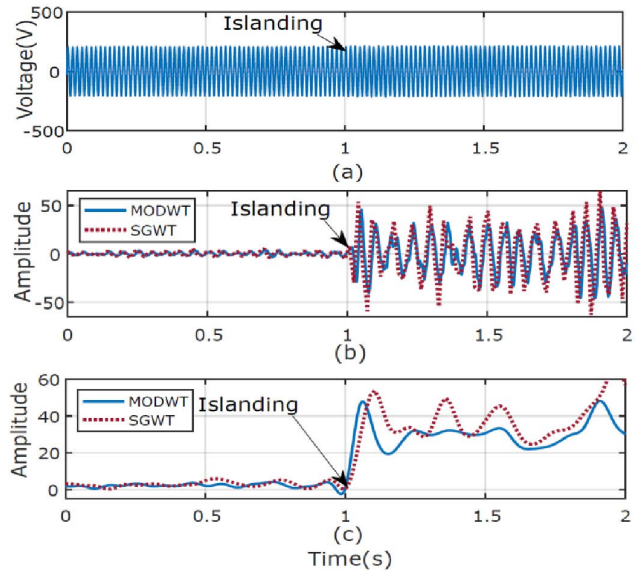
scheme is shown in FIGURE 1; the proposed hybrid test system is evaluated under wind velocity of 12m/s and irradiation of 1000 W/m². Maximum power is derived from the P.V. array through an independent PV-MPPT controller under rapidly varying irradiation and load resistance [20]. The voltage of the DC-link is controlled according to the output from PV-MPPT. Maximum power is derived from wind turbine-driven PMSGs using an optimal torque MPPT controller [21], reference torque is produced, and associated switching pulses are generated. Consequently, the wind side converter delivers maximum power to the DC-link, giving both power sources maximum power in all atmospheric conditions. The voltage and frequency needed to drive the utility and maintain the unity power factor are entirely controlled by GSC.PMSG and photovoltaic sources are rated at 8 kW and 100 kW, respectively [22].

B. PROCESS ALGORITHM OF THE PROPOSED METHODS

FIGURE 2 represents the flow chart of the process algorithm of the proposed methods. There will be no islanding detection in many passive approaches when the inverter output power equals the load power because this is counterproductive to the power system. We have monitored the voltage variations at PCC to overcome this kind of situation in our proposed techniques. Variations are attributed to the high switching frequency and voltage ripple as in the D.C. link. FIGURE 3(a) shows a voltage measured at the PCC, FIGURE 3(b) depicts the output waveform of the third level approximate coefficients of the MODWT technique. The coefficients are obtained using 'db4' as the mother wavelet and third-level approximation generated from the iterative operation of the SGWT technique. FIGURE 3(c) shows an islanding detection waveform (ISDW) from the mean of the upper envelope for the third-level approximate coefficients

TABLE 1. Different tested scenarios.

Scenario	Variation	No.of Tests Performed
Islanding		
Active power	$-20\%\,to+20\%$	20
Reactive power	$-2\%\,to+2\%$	20
Quality factor	1 to 2.5	05
Non-Islanding		
LLL Fault	$R_f = 1 - 75\Omega$	16
LL Fault	$R_f = 1 - 75\Omega$	16
LG Fault	$R_f = 1 - 75\Omega$	16
Load switching	10-108 kVA	21
Capacitor switching	10-108 kVAR	21
Loss of parallel feeder	1000-2000 MVA	05
Effect on System Parameters		
Transformer Rating	110-300 kVA	10
Hybrid DG power	25-220 kW	09
Noise	20-40 dB	21
Sampling frequency	1-3 kHz	03
Total Events (MODWT+ SGWT) 183+183=366		

FIGURE 4. Zero Power Deviation case (a) ISDW (b) Trigger signal.

in the SGWT and MODWT. There is a significant difference in ISDW magnitude before and after the islanding condition. The magnitude of the ISDW is compared with the threshold values for predetermined delay time; then, the islanding can be detected.

IV. RESULTS AND DISCUSSION

A wide variety of islanding and non-islanding cases are tested to evaluate the proposed algorithm's effectiveness. Table 1 presents the various scenarios and the number of tests performed in each scenario.

A. ISLANDING CASES

1) ISLANDING DETECTION WHEN ZERO-POWER MISMATCHED CONDITION

In this case, the proposed algorithm's performance is tested when the amount of D.G. power is equal to the load power. FIGURE 4(a) depicts ISDW with MODWT and SGWT when zero-power mismatched condition with a load quality factor is one (Q=1). FIGURE 4(b) shows the trigger signal. The breaker opens at one second and senses islanding after 0.3 sec of breaker opening. Before the breaker opens, the amplitude variance of the detection waveform (ISDW) is less than the pre-defined threshold. After the breaker opens, the amplitude variation of the detection waveform (ISDW) is more than the pre-defined threshold value with a delay; with this information, islanding could be detected. The proposed method can detect islanding even under zero power mismatch conditions. So, the NDZ of the proposed algorithm is almost zero.

2) VARIATION IN LOAD QUALITY FACTOR

As per IEEE std, the range of load quality factors considered during islanding detection is between 1 and 2.5. Using MODWT and SGWT, FIGURE 5(a) illustrated the impact of a variable load quality factor on ISDW in the presence of a zero-power mismatch. The gap between the grid-connected and islanding ISDW magnitudes is minimized by increasing the load quality factor. Higher' Q' indicates an increased
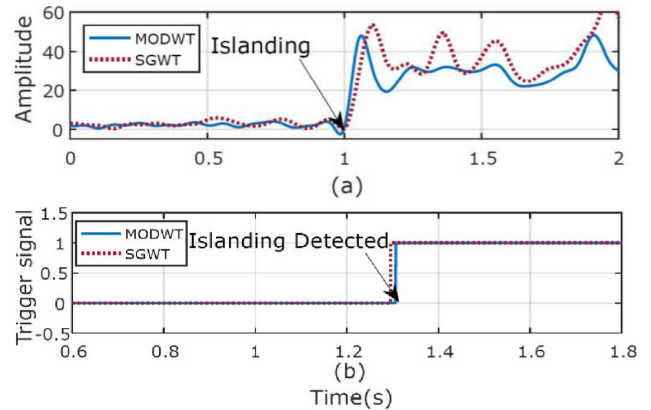
load of reactance, which will decrease the number of voltage and current waveform frequency oscillations after islanding. A similar phenomenon for all other islanding situations is found in the ISDW. FIGURE 5(b) showed the trigger signal in MODWT and SGWT. The proposed algorithm assures the accurate detection of islanding even under zero power mismatch conditions. So, the NDZ of the proposed algorithm is null.

3) REAL POWER MISMATCH

FIGURE 6(a) and 7(a) showed the ISDW variations for real power imbalances of the D.G. power and load power, considering the MODWT and the SGWT. The ISDW magnitude is greater than the threshold level after the breaker opening. Therefore both the transformation techniques detect the islanding condition shown in FIGURE 6(a) and 7(a). The D.G. capacity is greater than the load capacity if there is a positive real power imbalance. Real power deviations are considered to increase and decrease cases by changing real power from 2% to 20%. If the power imbalance varies by more than 20%, the voltage levels would be divergent from the region of NDZ—accordingly, the maximum imbalance, which we estimated to be about 20%. FIGURE 6(b) and 7(b) showed the trigger signal for real power mismatches in the MODWT and the SGWT.

4) REACTIVE POWER MISMATCH

FIGURE 8(a) and 9(a) showed the ISDW signal for reactive power imbalance for inductive and capacitive-load. Whenever the breaker opens at 1.0 seconds, the magnitude of the detection signal (ISDW) increases and crosses the threshold level. The algorithm determines islanding condition is present. Suppose there is a positive mismatch; it implies that the capacitive demand becomes less than the inductive and conversely. For reactive power analysis, 0.2% to 2% of the total reactive power variance is considered. If the reactive power imbalance extends predefined limits of +2% and −2%, the frequency deviates from the NDZ.
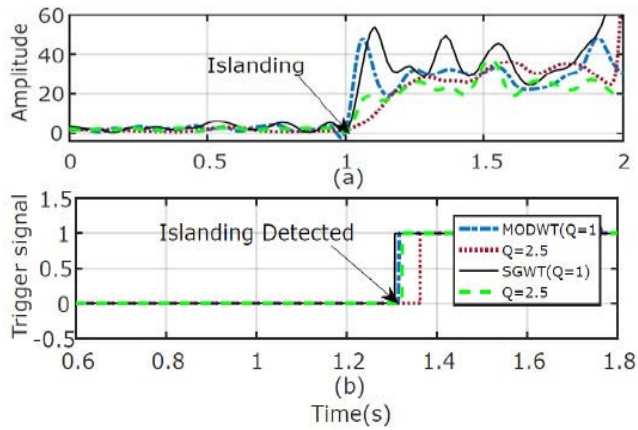
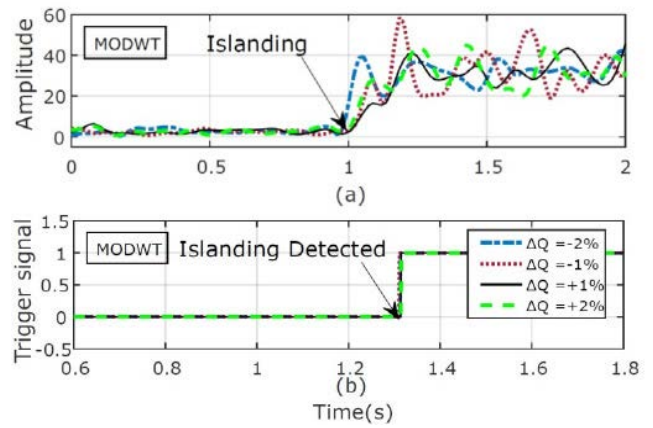**FIGURE 5.** (a) ISDW for different quality factors utilizing MODWT & SGWT (b) Trigger signal.

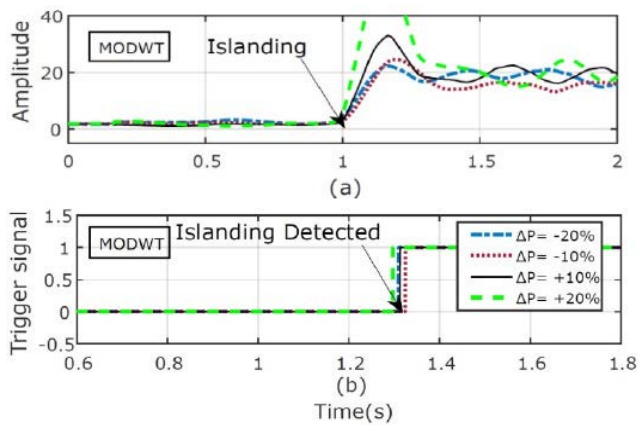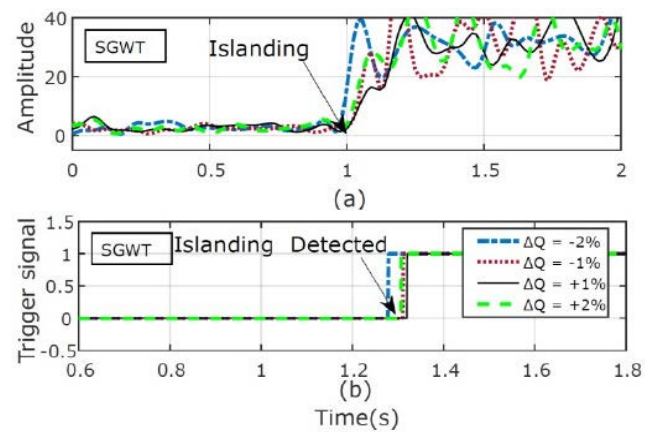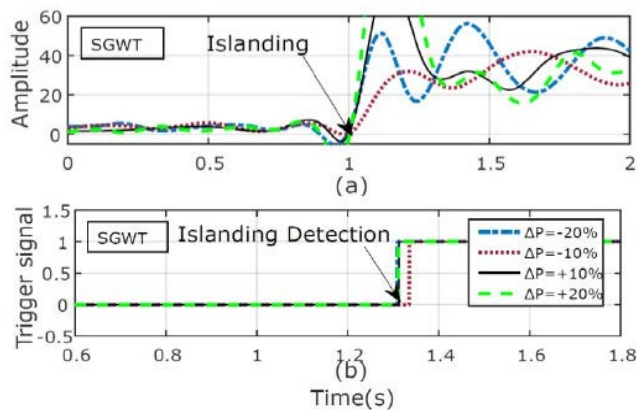**FIGURE 6.** (a) ISDW applying MODWT for different real power mismatches (b) Trigger signal.

FIGURE 7. (a) ISDW using SGWT for varying real power of the load (b) Trigger signal.

FIGURE 8(b) and 9(b) showed the trigger signal for reactive power imbalance in the MODWT and the SGWT.

B. NON-ISLANDING CASES
Different faults, loss of parallel feeder, load and capacitor switching, etc., are the various possible non-islanding

FIGURE 8. (a) ISDW applying MODWT for different load reactive powers (b) Trigger signal.

FIGURE 9. ((a) ISDW applying SGWT for different reactive power mismatches (b) Trigger signal.

scenarios that can cause the false detection of islanding. All of these non-islanding scenarios are being tested to validate the effectiveness of the proposed islanding detection technique.

1) SHORT CIRCUIT FAULTS
Different kinds of short-circuit faults are simulated, such as three-phase fault (LLL), two-phase fault (L.L.), phase-ground fault (L.G.), respectively. The circuit breaker in the parallel feeder is tripped within 0.02s, thus clearing the fault. Each case fault resistance is varied from 1 to 75 ohm. FIGURE 10(a) and 10(b) shows ISDW detection signal for LLL, L.L., L.G. faults, respectively. The detection signal settling time was small relative to the pre-defined detection delay in all kinds of faults, so no false detection is triggered, as shown in FIGURE 10(c). There is a peak in the waveform of ISDW, it saturates very rapidly, but at the end of the method, the pre-defined time delay is used to divert incorrect trips from non-islanding situations. The maximum time delay for various fault resistances in LLL, L.L., L.G. faults is shown in Table 2. It is observed that the maximum time delay as fault
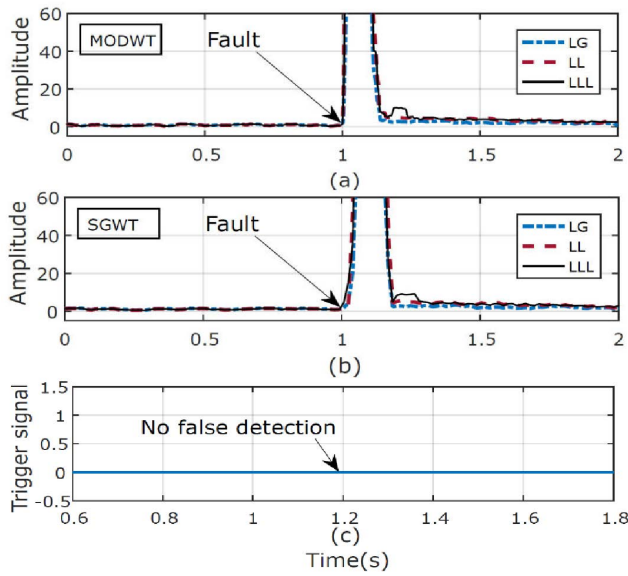
FIGURE 10. ISDW using (a) MODWT (b) SGWT for different fault cases (c) Trigger signal.
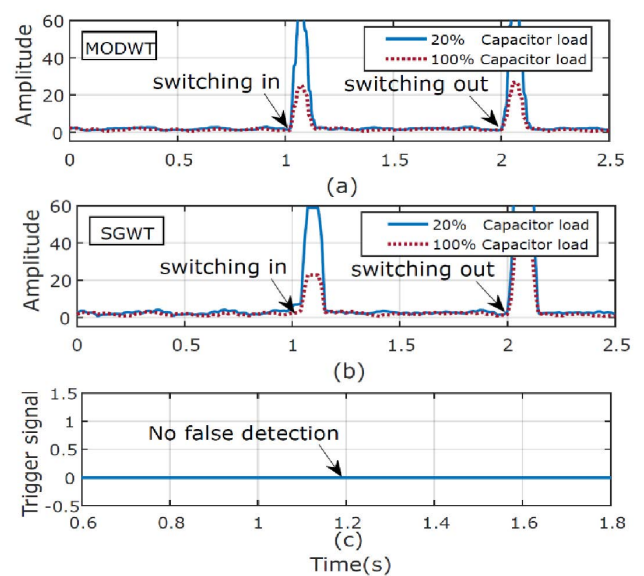

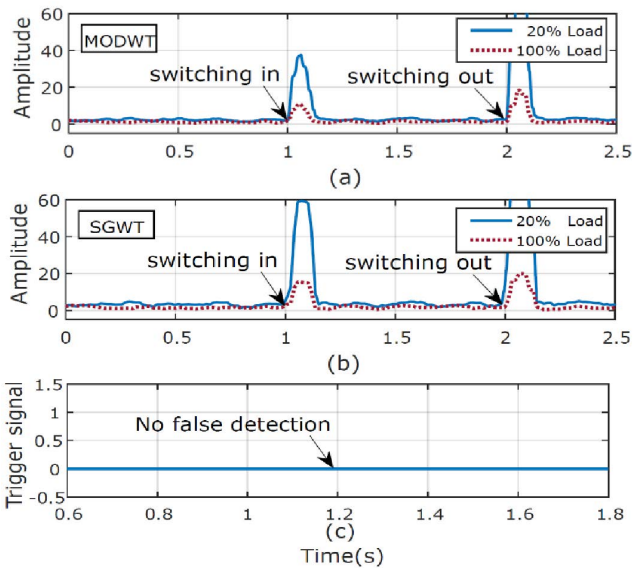**FIGURE 11.** ISDW using (a) MODWT (b) SGWT for load switching cases, (c) Trigger signal.

FIGURE 12. ISDW using (a) MODWT (b) SGWT for capacitor bank switching cases, (c) Trigger signal.

resistance increases, maximum delay decreases in both the MODWT and the SGWT decompositions.

2) LOAD SWITCHING

In this case, load switching ON and OFF are considered. The load is switched ON at 1.0 sec, and it is increased with steps of 10% up to 100% with step duration of 0.02 sec, and the same stepwise load is removed from 100% to 10% from 2.0 sec onwards with the same step duration of 0.02 sec. The islanding detection signals using MODWT and SGWT are showed in FIGURE 11(a) & 11(b) for 20% and 100% of load switching. There was no false islanding detection

for both these cases because the ISDW signal is flat during load switching, which means the detection signal fell to normal values since the pre-defined delay elapsed, as shown in FIGURE 11(c).

3) CAPACITOR BANK SWITCHING

The capacitor bank is switched ON at 1.0 sec, and it is increased with steps of 10% up to 100% with a step duration of 0.02 sec. Similarly, the capacitor banks are removed stepwise from 100% to 10% from 2.0 sec onwards with the same step duration of 0.02 sec. The islanding detection signals using MODWT and SGWT are shown in FIGURE 12(a) & 12(b) for 20% and 100% of capacitor bank switching. In the entire capacitor bank switching cases, there is a peak in the MODWT and SGWT waveforms. It saturates very quickly, so, by using a proper time delay and threshold, false tripping is avoided, as shown in FIGURE 12(c).

C. EFFECT ON SYSTEM PARAMETERS

1) VARIATION IN THE HYBRID DG POWER

The inverter output and hybrid D.G. power are varied between 25 and 220 kW. The zero-power mismatch islanding situation is considered for various D.G. ratings using a load quality factor of 2.5. Table 3 illustrates the impact of varying D.G. capacity in all islanding and grid-connected scenarios about ISDW magnitudes. In the grid-connected situation, the magnitude of ISDW was constantly well below the threshold, but in the islanded case was continually over the threshold level. This indicates here that the hybrid D.G.'s capacity does not limit the technique's performance.

2) CHANGE IN TRANSFORMER RATING

To assess the efficacy of the proposed technique, the KVA rating of the distribution transformer is adjusted in

TABLE 2. Effect of fault resistance on time delay.

Fault Type	Maximum delay (MODWT/SGWT) in sec			
	Rf=1	Rf=25	Rf=50	Rf=75
LLL	0.16/0.218	0.14/0.18	0.13/0.144	0.12/0.13
LL	0.14/0.16	0.12/0.15	0.12/0.136	0.11/0.12
LG	0.12/0.14	0.11/0.12	0.1/0.115	0.98/0.10

TABLE 3. Impact of variation in the D.G. power.

DG power (kW)	Maximum amplitude before islanding (V)		Minimum amplitude after islanding (V)	
	MODWT	SGWT	MODWT	SGWT
25	2.86	3	29.2	37.5
50	2.72	2.75	27.4	35.9
100	2.7	2.9	19	25.9
150	2.89	2.4	12.35	14.59
200	3.12	3.68	17.5	20.4
220	3.31	3.83	18.3	22.3

FIGURE 13. ISDW for (a) MODWT (b) SGWT for different sampling frequencies.

TABLE 4. Effect of change in hybrid DG power.

Transformer(KVA)	Maximum amplitude before islanding (V)		Minimum amplitude after islanding (V)	
	MODWT	SGWT	MODWT	SGWT
110	1.9	1.52	18.4	25.4
150	2.7	2.9	19	25.9
200	2.25	2.42	21.2	28.9
250	2.12	1.82	24.9	33.6
300	1.89	1.6	29.3	42.7

TABLE 5. Impact of different Noise levels.

Mode	No of Cases verified	No of the cases verified MODWT/SGWT			
		20dB	30dB	40dB	Accuracy (%)
Islanding	15	15/15	15/15	15/15	100/100
Non-Islanding	6	6/6	6/6	6/6	100/100

of noises. The minimum values of ISDW for all islanding cases were always above the threshold, and the time delay for non-islanding was consistently below the optimum time delay value.

4) SAMPLING FREQUENCY
Various sample frequencies are used to evaluate the suggested algorithm's performance. A load quality factor (Q=2.5) is utilised to simulate a zero-power mismatch islanding situation using a variety of sampling frequencies. FIGURE 13 shows a variety of ISDW versions. Because the ISDW levels were consistently below and slightly over the threshold in both the grid-connected and islanding situations, it suggests that the recommended approach is unaffected by frequency changes in its ability to identify islanding.

D. HIL IMPLEMENTATION
The simulation results were validated using the Opal RT OP5700 HIL Simulator, RT-LAB, MSOX3014T, PCB-E06-0560. The PCB is used to communicate between the simulation and the real-time controller via analog outputs and digital inputs. The machine and controller are placed in OPAL-RT to ensure that the system runs correctly. The high-speed nano to microsecond OPAL-RT sample rate transforms this system into a dynamically real-time system. The user PC is in charge of the RT-digital LAB's simulator (RTDS) commands. RT-LAB is used to edit, build, load, and operate the prototype.

1) ISLANDING DETECTION WHEN ZERO-POWER MISMATCHED CONDITION (ISLANDING EVENT)
In this case, the proposed algorithms' real-time validation is evaluated when the power from the D.G. matches the load power. FIGURE 15(a) & 15(b) illustrates ISDW with MODWT and SGWT in the presence of a zero-power mismatch and shows the trigger signal. The breaker opens at a time of 6.0 seconds and detects islanding within 0.3 seconds of opening.

both islanding and grid-connected situations. The islanding behaviour of transformers with varying kVA ratings is investigated using a load quality factor (Q=2.5) and no power mismatch. Table 4 shows the influence of different ratings of transformers with ISDW magnitudes in islanding and grid-connected situations. The ISDW for grid-connected (before islanding) was found to be continuously below the threshold due to the effect of grid stabilization. The ISDW value decreases as the rating of the transformer increases. The ISDW for islanding was always above the threshold due to the transformer's impedance on the load. This increase of impedance results in changes in the PCC voltage signal that raises the ISDW amplitude.

3) SIGNAL-TO-NOISE RATIO (SNR)
Distortion is introduced in the PCC voltage signal with white Gaussian noise to test the proposed system's ability. The noise levels, i.e., SNR = 20, 30, and 40 dB, are applied to the PCC voltage signal. In Table 5, it can be noticed that the suggested approach has better accuracy against various types
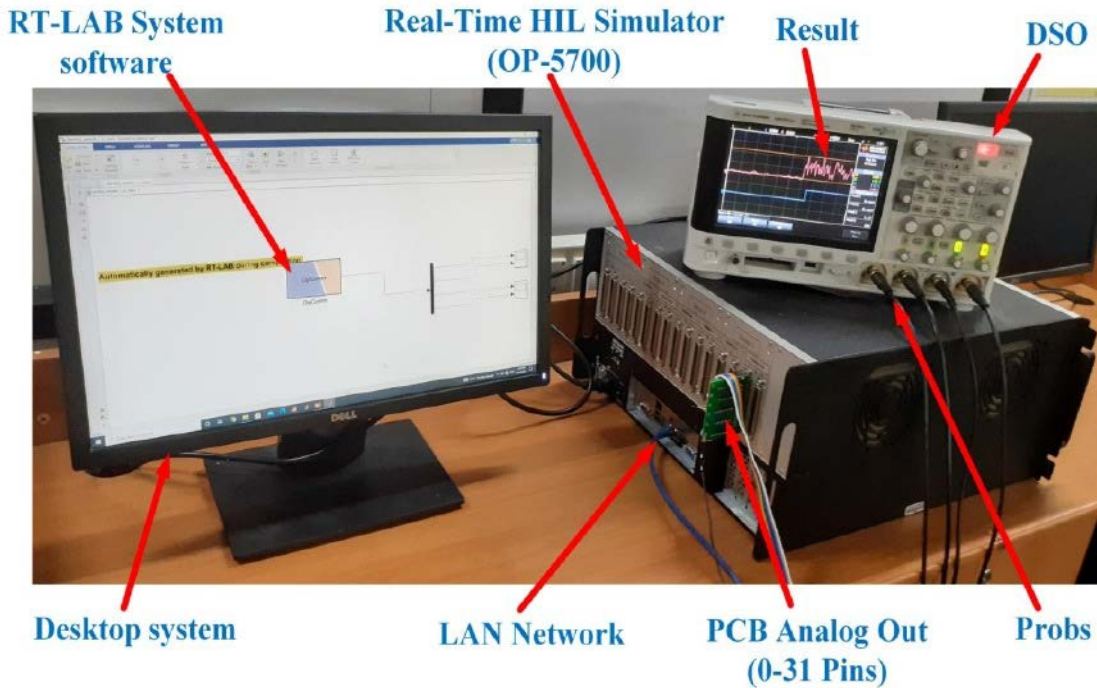
FIGURE 14. Real-Time (RT) HIL setup.

TABLE 6. Comparison of the proposed approach with other signal processing techniques "N.C." = Not considered. "V.F." = Verified.

Technique	Zero power mismatch	Load quality factor	Short circuit faults	Noise	Change in DG rating	Sampling frequency	Need of classifier
DWT[8]	V.F.	N.C.	N.C.	Fails	N.C.	N.C.	YES
EMD[10]	N.C.	N.C.	V.F.	V.F.	N.C.	N.C.	YES
ST[6]	N.C.	N.C.	V.F.	V.F.	V.F.	N.C.	YES
WPT[9]	V.F.	V.F.	N.C.	V.F.	V.F.	N.C.	YES
TMF[13]	Fails	N.C.	N.C.	V.F.	N.C.	N.C.	No
OEMD[11]	V.F.	N.C.	N.C.	V.F.	N.C.	N.C.	No
MP[15]	Fails	V.F.	N.C.	N.C.	N.C.	N.C.	No
MM[14]	V.F.	N.C.	Fails	N.C.	N.C.	N.C.	No
VMD[12]	Fails	V.F.	N.C.	V.F.	N.C.	N.C.	No
Proposed techniques	**V.F.**	**V.F.**	**V.F.**	**V.F.**	**V.F.**	**V.F.**	**No**

2) 3-PHASE FAULT CONDITION (NON-ISLANDING EVENT)

FIGURE 16(a) & 16(b) shows the real-time validation of the non-islanding event (3-Phase fault) ISDW signal. The proposed methods have a distinct ability to separate the islanding and non-islanding events, which is evident in a real-time environment. FIGURE 14 illustrates the arrangement of the real-time results.

E. COMPARISON

This section compares the proposed approaches with several other signal processing islanding detection algorithms found in the literature, as summarized in Table 6. The VMD, TMF, and M.P. approaches are not accurate regarding low power mismatch and they are not considered fault conditions for validating non-islanding events. Although DWT and OEMD

minimize the NDZ, the load and capacitor switching and fault cases have not been validated. Most approaches do not consider changes in D.G. capability and noise, which are critical for identifying islanding. While the TMF, MP, OEMD, MM, and VMD approaches do not need a classifier, they may struggle to differentiate between islanding and non-islanding incidents under various operating settings. Furthermore, the faulty situations that are very important to island identification have not been mentioned in the DWT, WPT, OEMD, TMF, and VMD methods. Many islanding detection algorithms have not considered non-islanding cases like load & capacitor switching and short-circuit faults. On the other hand, the proposed algorithm overcomes these drawbacks. The power imbalance is among the most key indicators of a detection approach. To prove the competence of the proposed
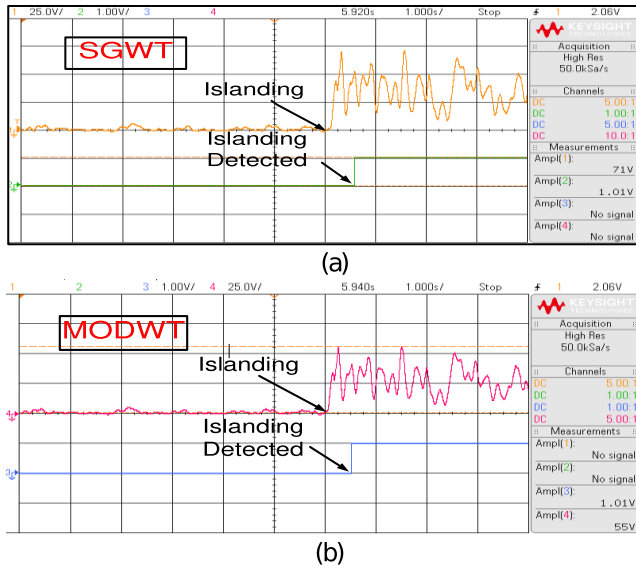
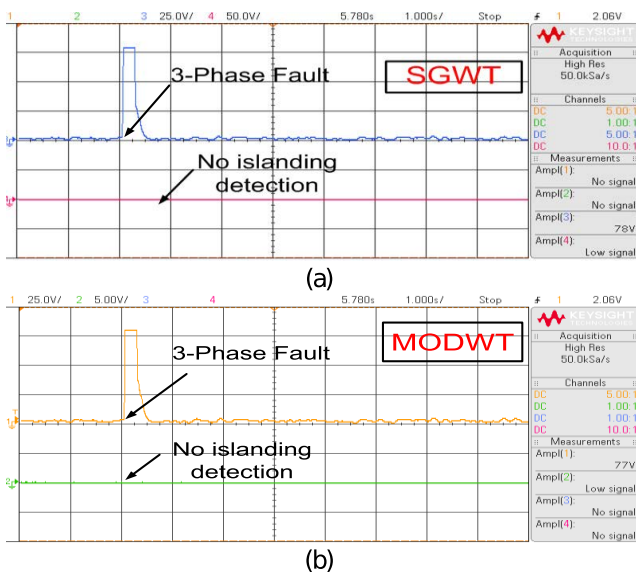**FIGURE 15.** Zero Power mismatch (ISDW) (a) SGWT (b) MODWT.

FIGURE 16. 3-Phase fault (ISDW) (a) SGWT (b) MODWT.

FIGURE 17. Performance assessment of proposed methods with DWT (a) Real power imbalance (b) Reactive power imbalance.

methods, real and reactive power imbalance cases among the load and the D.G. are considered.

The power imbalance is among the most critical indicators of an islanding detection approach. To prove the effectiveness of the proposed methods, real and reactive power imbalance cases among the load and the DG are identified for the three approaches' comparison purposes. FIGURE 17 illustrates the comparison between the three methods of their detection speed with the active and reactive power mismatch. The figure shows that the proposed MODWT and SGWT detection methods are capable of performing faster islanding detection compared to the existing ones.
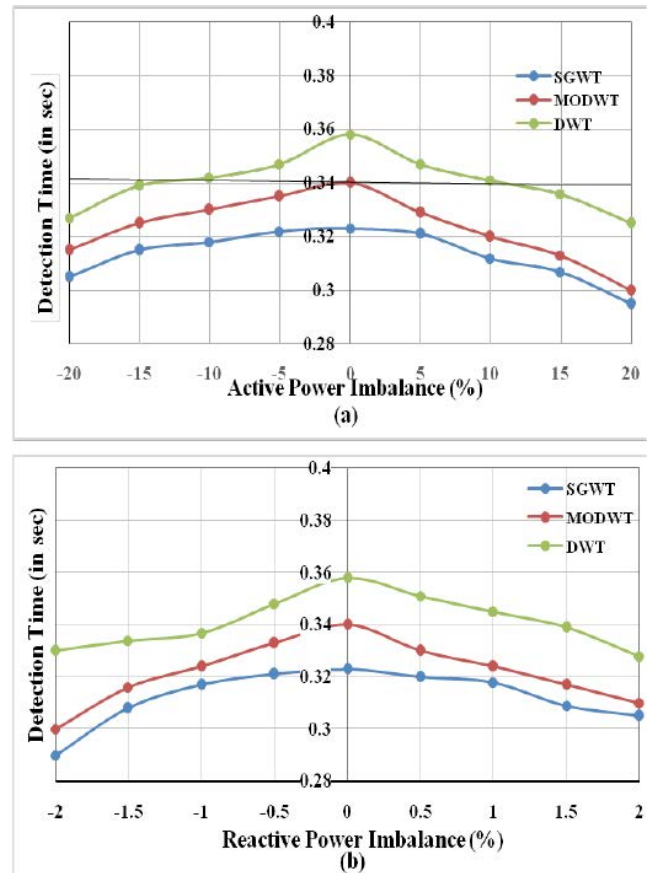
V. CONCLUSION

This paper proposes the SGWT and MODWT passive islanding detection techniques. The proposed methods detected islanding nearly at 0.3 seconds. The SGWT has some merits, such as low memory requirement, less computing time, and good performance. Further, the SGWT's reduced computing time encourages voluminous data processing more quickly. Similarly, the MODWT free down sampling gives the correct location of events, eliminating the down-sampling, which overcomes the range of the signal length. The proposed techniques were validated for various islanding cases, and they are independent of the system parameters and effectively separate islanding and non-islanding situations without any requirement of a classifier. Additionally, these methods give optimum threshold value regardless of ISDW variations induced by different non-islanding conditions. The proposed methodologies may be employed in online networks to detect islanding effectively.

REFERENCES

[1] X. Chen and Y. Li, "An islanding detection algorithm for inverter-based distributed generation based on reactive power control," *IEEE Trans. Power Electron.*, vol. 29, no. 9, pp. 4672–4683, Sep. 2014.

[2] P. Bezawada, P. O. Yeddula, and V. R. Kota, "A novel time-domain passive islanding detection technique for grid-connected hybrid distributed generation system," *Arabian J. Sci. Eng.*, vol. 46, no. 10, pp. 9867–9877, Oct. 2021.

[3] G. Bayrak and E. Kabalci, "Implementation of a new remote islanding detection method for wind–solar hybrid power plants," *Renew. Sustain. Energy Rev.*, vol. 58, pp. 1–15, May 2016.

[4] R. V. Reddy and E. S. Sreeraj, "A feedback-based passive islanding detection technique for one-cycle-controlled single-phase inverter used in photovoltaic systems," *IEEE Trans. Ind. Electron.*, vol. 67, no. 8, pp. 6541–6549, Aug. 2020.

[5] K. H. Reddy, "Modified SRFPLL harmonic support island detection in integrated electric grid," *Electr. Eng.*, vol. 104, pp. 1305–1315, Sep. 2021.

[6] P. K. Dash, M. Padhee, and T. K. Panigrahi, "A hybrid time–frequency approach based fuzzy logic system for power island detection in grid connected distributed generation," *Int. J. Electr. Power Energy Syst.*, vol. 42, no. 1, pp. 453–464, Nov. 2012.

[7] P. P. Mishra and C. N. Bhende, "Islanding detection using sparse S-transform in distributed generation systems," *Electr. Eng.*, vol. 100, no. 4, pp. 2397–2406, Dec. 2018.

[8] H. Shayeghi and B. Sobhani, "Zero NDZ assessment for anti-islanding protection using wavelet analysis and neuro-fuzzy system in inverter based distributed generation," *Energy Convers. Manage.*, vol. 79, pp. 616–625, Mar. 2014.

[9] H. T. Do, X. Zhang, N. V. Nguyen, S. Li, and T. T. Chu, "Passive-islanding detection method using the wavelet packet transform in grid-connected photovoltaic systems," *IEEE Trans. Power Electron.*, vol. 39, no. 10, pp. 6955–6967, Oct. 2016.

[10] M. Mishra, M. Sahani, and P. K. Rout, "An islanding detection algorithm for distributed generation based on Hilbert–Huang transform and extreme learning machine," *Sustain. Energy, Grids Netw.*, vol. 9, pp. 13–26, Mar. 2017.

[11] H. R. Singh, S. R. Mohanty, N. Kishor, and K. A. Thakur, "Real-time implementation of signal processing techniques for disturbances detection," *IEEE Trans. Ind. Electron.*, vol. 66, no. 5, pp. 3550–3560, May 2019.

[12] S. Salimi and A. Koochaki, "An effective method for islanding detection based on variational mode decomposition," *Electrica*, vol. 19, no. 2, pp. 135–145, Jul. 2019.

[13] R. Dubey, M. Popov, and S. R. Samantaray, "Transient monitoring function-based islanding detection in power distribution network," *IET Gener., Transmiss. Distrib.*, vol. 13, no. 6, pp. 805–813, Mar. 2019.

[14] M. A. Farhan and K. S. Swarup, "Mathematical morphology-based islanding detection for distributed generation," *IET Gener., Transmiss. Distrib.*, vol. 10, no. 2, pp. 518–525, 2016.

[15] S. Agrawal, S. Patra, S. R. Mohanty, V. Agarwal, and M. Basu, "Use of matrix-pencil method for efficient islanding detection in static DG and a parallel comparison with DWT method," *IEEE Trans. Ind. Electron.*, vol. 66, no. 11, pp. 8937–8946, Nov. 2019.

[16] S. Upadhyaya, C. N. Bhende, S. Mohanty, and R. Pati, "Evaluation of power quality disturbance in PV-connected IEEE-14 bus system using lifting-based wavelet transform and random forest," *Electr. Eng.*, vol. 104, pp. 2345–2354, Jan. 2022.

[17] S. Upadhyaya and S. Mohanty, "Fast methods for power quality analysis," *Int. J. Emerg. Electr. Power Syst.*, vol. 18, no. 5, pp. 1–17, Oct. 2017.

[18] S. Li, T. A. Haskew, R. P. Swatloski, and W. Gathings, "Optimal and direct-current vector control of direct-driven PMSG wind turbines," *IEEE Trans. Power Electron.*, vol. 27, no. 5, pp. 2325–2337, May 2012.

[19] Y. Gui, X. Wang, and F. Blaabjerg, "Vector current control derived from direct power control for grid-connected inverters," *IEEE Trans. Power Electron.*, vol. 34, no. 9, pp. 9224–9235, Sep. 2019.

[20] T. K. Soon and S. Mekhilef, "A fast-converging MPPT technique for photovoltaic system under fast-varying solar irradiation and load resistance," *IEEE Trans. Ind. Informat.*, vol. 11, no. 1, pp. 176–186, Feb. 2015.

[21] M. Yin, W. Li, C. Y. Chung, L. Zhou, Z. Chen, and Y. Zou, "Optimal torque control based on effective tracking range for maximum power point tracking of wind turbines under varying wind conditions," *IET Renew. Power Gener.*, vol. 11, no. 4, pp. 501–510, Mar. 2017.

[22] B. Pangedaiah, Y. P. Obulesu, and V. R. Kota, "A new architecture topology for back to back grid-connected hybrid wind and PV system," *J. Electr. Eng. Technol.*, vol. 16, no. 3, pp. 1457–1467, May 2021.

B. PANGEDAIAH received the B.E. degree in electrical engineering from Andhra University, in 2006, and the M.Tech. degree in power systems and the Ph.D. degree from Jawaharlal Nehru Technological University, Andhra Pradesh, India, in 2011 and 2022, respectively. He is currently working as a Senior Assistant Professor with the Department of Electrical and Electronics Engineering, Lakireddy Bali Reddy College of Engineering, Mylavaram, Andhra Pradesh. His research interests include islanding detection, renewable sources grid integration, and signal processing techniques.

P. L. SANTOSH KUMAR REDDY received the B.Tech. degree in electrical engineering from the Sri Prakash College of Engineering, in 2016, and the M.Tech. degree in power electronics and drives from the Lakireddy Bali Reddy College of Engineering, in 2018. He is currently pursuing the Ph.D. degree with the School of Electrical Engineering, Vellore Institute of Technology, Vellore, India. His research interests include power electronics, high step-up DC-DC boost converter topologies, multi-port DC-DC converters, and renewable energy source grid integration.

Y. P. OBULESU received the B.E. degree in electrical engineering from Andhra University, in 1995, the M.Tech. degree in machine drives and power electronics from the Indian Institute of Technology, Kharagpur, in 1998, and the Ph.D. degree from Jawaharlal Nehru Technological University, Andhra Pradesh, India, in 2006. He is currently working as a Professor with the School of Electrical Engineering, Vellore institute of technology, Vellore, India. His research interests include power converters, electric vehicles, micro e-mobility control of electrical drives, EV fast charging, battery management systems, DC microgrids, DC distribution, harmonic mitigation and power quality, and AI and ML techniques.

VENKATA REDDY KOTA (Senior Member, IEEE) received the Ph.D. degree in electrical engineering with JNTUK, Kakinada, Andhra Pradesh, India, in 2012. He is currently working as a Professor with the Department of Electrical and Electronics Engineering, Jawaharlal Nehru Technological University, Kakinada. His research interests include special electrical machines, electric drives, FACTS, and custom power devises and power quality. He is a member of the Institution of Engineers, India, and the Indian Society for Technical Education. He was a recipient of the "Tata Rao Prize" from the Institution of Engineers, in 2012. He was also a recipient of the "IEI Young Engineers Award" from the Institution of Engineers, in 2013.

MAMDOUH L. ALGHAYTHI (Member, IEEE) received the B.S. degree in electrical engineering from Jouf University, Sakaka, Saudi Arabia, in 2012, the M.S. degree in electrical engineering from Southern Illinois University, Carbondale, IL, USA, in 2015, and the Ph.D. degree in electrical engineering from the University of Missouri, Columbia, MO, USA, in 2020. He is currently an Assistant Professor with the Department of Electrical Engineering, Jouf University. His current research interests include power electronics, renewable energy systems, high step-up DC-DC converters, microgrids, and power converters.

• • •